

## Tribological performance evaluation of coated steels with TiNbCN subjected to tribo-chemical wear in Ringer's solution

J. Caballero-Gómez<sup>a</sup>, J.C. Caicedo<sup>b</sup> and W. Aperador<sup>a</sup>

<sup>a</sup>*Volta Research Group,*

*Universidad Militar Nueva Granada, Bogotá-Colombia.*

<sup>b</sup>*Tribology Polymers, Powder Metallurgy*

*and Processing of Solid Recycled Research Group Universidad del Valle, Cali, Colombia,*

*e-mail: g.ing.materiales@gmail.com*

Received 5 May 2015; accepted 2 December 2015

With the aim of generating solutions against the deterioration of the joint prostheses, it was studied the tribo-corrosive behavior of titanium niobium carbonitride (TiNbCN) deposited on stainless steel AISI 316 LVM using the technique of magnetron sputtering physical vapor deposition. The tests were performed in a balanced saline solution (Ringer's solution) which represents the characteristics of the body fluids, using an equipment where the micro-abrasive wear is generated by the contact of micro particles in the system; the micro-abrasion-corrosion mechanism is described by means of the incorporation of an electrochemical cell consisting of three electrodes. Both the substrate and the coating, were subjected to micro-abrasive wear simultaneously with the electrochemical tests of Tafel polarization curves and electrochemical impedance spectroscopy (EIS); subsequently of the tests, the specimens were analyzed by optical microscopy and scanning electron microscopy characterizing the surface morphology. It was observed that the coating presents an increase in its corrosion and wear resistance with the presence of a simulated biological fluid.

**Keywords:** Micro-abrasion; coating; AISI 316 LVM; wear; corrosion.

PACS: 87.80.Ek; 81.15.-z; 75.20.En; 46.55.+d; 82.45.Bb.

### 1. Introduction

Biomaterials are designed to interact with biological systems, in order to replace or repair tissues, organs or functions of the human body [1-3]. The materials used in orthopedic surgery are one of the branches with important applications, since the different joints of the human body suffer deterioration over the time (approximately 108 load cycles in 70 years). Hence, the mechanical properties decrease as a consequence of the joint wear and degradation in connective tissues such as cartilage and tendons [3,4]. In addition, degenerative diseases such as osteoporosis, osteoarthritis, bone loss and others, increase the bone fractures in elderly; it is estimated that more than fifty percent of all people over 60 will suffer these diseases and together with the increased life expectancy young people are using joint prostheses. Therefore, the use of prostheses has extended, demanding a longer service life for these elements, which makes their substitution necessary. These substitutions are technically very complicated and with an unpredictable clinical result in some cases [5]. In Colombia, about 20,000 operations of hip and knee joints are performed annually where ten years after implantation, the patient begins to feel pain and discomfort, losing mobility and even has to undergo another surgery. The incidence of a second and even a third surgery is frequent, which has as aggravating the proliferation of the tissue bone area and a poor life quality, it justifies the necessity of develop biomaterials with better properties that ensure a longer service time [6].

The orthopedic surgery has used different materials combinations such as metallic, polymers and ceramics with the aim of reducing the harmful effects and improving the per-

formance of the elements which are made the joint replacements [7-11]. In general terms, most joint implants involves a combination of a metallic material against a component of ultra-high molecular weight polyethylene (UHMWPE), although this decreases the service life of the implant due to high wear that polymeric materials exhibit [12,13]. As alternative of the metal-on-polymer (MoP), it have been raised implants metal-on-metal (MoM) and ceramic-on-ceramic (CoC) which have gained acceptance owing to its high resistance to wear [14-16]. However, each combination presents some disadvantages, the (MoM) generate biocompatibility problems when they are used as permanent implants due to the ion release to the surrounding tissues [17-20]; and the (MoC) despite of minimize the wear problem largely, they suffer the possibility to have a catastrophic failure by fracture of the implant due to the fragility of these materials [10-11].

In these circumstances, an alternative to improve the implants are the surface modifications of the conventional materials using protective coatings. As these coatings have been developed in order to increase the useful life of the substrate by the enhancement of the properties against wear and corrosion [21,22]. Different coatings based on borides, carbides, and nitrides and transition metals have been used to enhance the tribological properties of tools. Furthermore, they have used in other applications as biomaterials due to their biocompatibility and affordable price, being the best known the titanium nitrides [20-22]. One interesting alternative of these coatings is the titanium niobium carbonitride (TiNbCN), which is already being used as a biomaterial but there are few studies regarding their tribological properties [23].

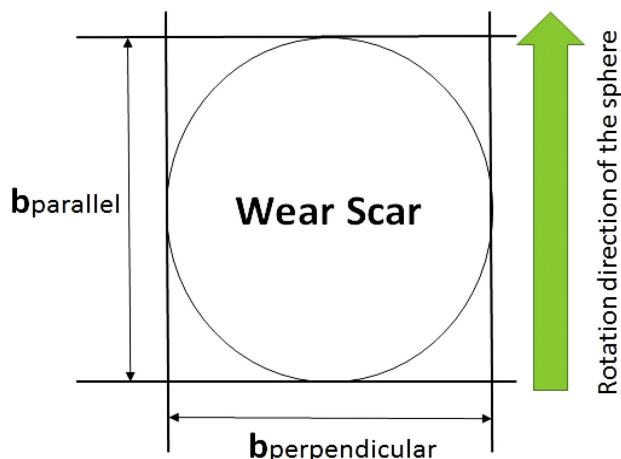


FIGURE 1. Measurement on wear scar.

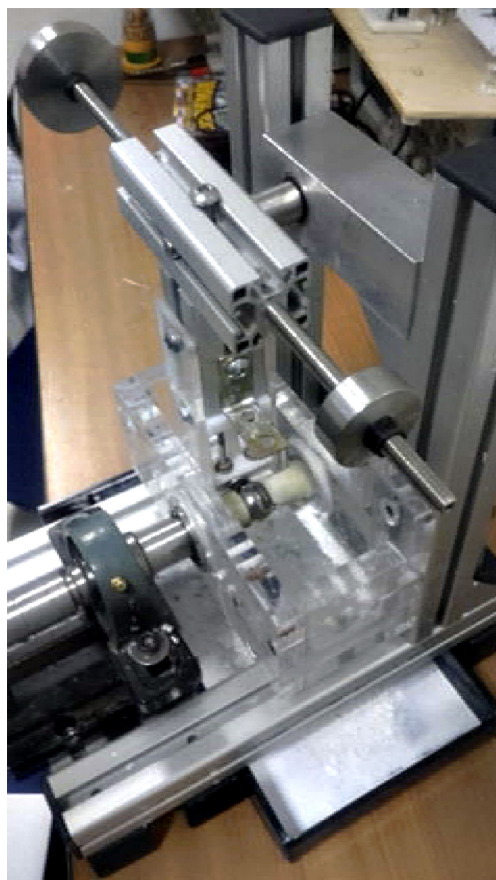


FIGURE 2. Micro-abrasion-corrosion equipment.

The aim of this work was the evaluation of the corrosive and tribological properties by means of micro-abrasion-corrosion test on stainless steel (AISI 316 LVM) coated with TiNbCN using the technique of magnetron sputtering physical vapor deposition (PVD) for future applications in the bio-engineering field.

## 2. Micro-abrasion wear calculation method

In the deterioration of biomaterials studies, the effect of abrasive wear generated by micro particles is normally ignored, due to the tribological variables involved in a biological system are misunderstood; nevertheless, this effect is important in the wear mechanism [7,24]. In this paper the calculations were done using a mathematical model that relates the dimensions of the wear track with a loss volume rate and a wear constant [26-28]. Therefore, after each test were taken parallel and perpendicular measurements of the generated wear scar according to the rotation of the sphere and then determine their average as shown in the Fig. 1.

In this type of test the wear volume is given by:

$$V = \frac{\pi b^4}{64R} \quad \text{for } b \ll R \quad (1)$$

Where  $b$  the crater diameter and  $R$  the sphere radius. Taking into account the Archard wear law is obtained that the volume of wear  $V$  is [27,28]:

$$V = KSN \quad (2)$$

Where:

- $K$  wear constant
- $S$  sliding distance.
- $N$  applied load.

By equating Eqs. (1) and (2) wear constant is described as:

$$K = \frac{\pi b^4}{64R} \cdot \frac{1}{SN} \quad (3)$$

## 3. Experimental detail

The test were performed in an equipment that has a specimen holder attached to a lever arm, which rotates on its pivot controlling the load on the specimen upon contact with the sphere by the movement of a dead weight and a counter weight. The ball is fixed between two coaxial shafts supported on bearings, when one of them is driven by DC motor with encoder to ensure the speed and number of revolutions of test. In order to observe the micro-abrasive process is provided to the system abrasive particles suspended in a container with a magnetic stirrer and a peristaltic pump controlled manually (see Fig. 2).

On the other hand, for the study of the corrosive phenomena it was adapted to the equipment a potentiostat that contains an electrochemical cell composed by: reference electrode - RE (Ag/AgCl), auxiliary electrode - AE (Platinum wire) and the specimen as a working electrode - WE. The electrodes are immersed in the solution of interest which acts as electrolyte (see Fig. 3).

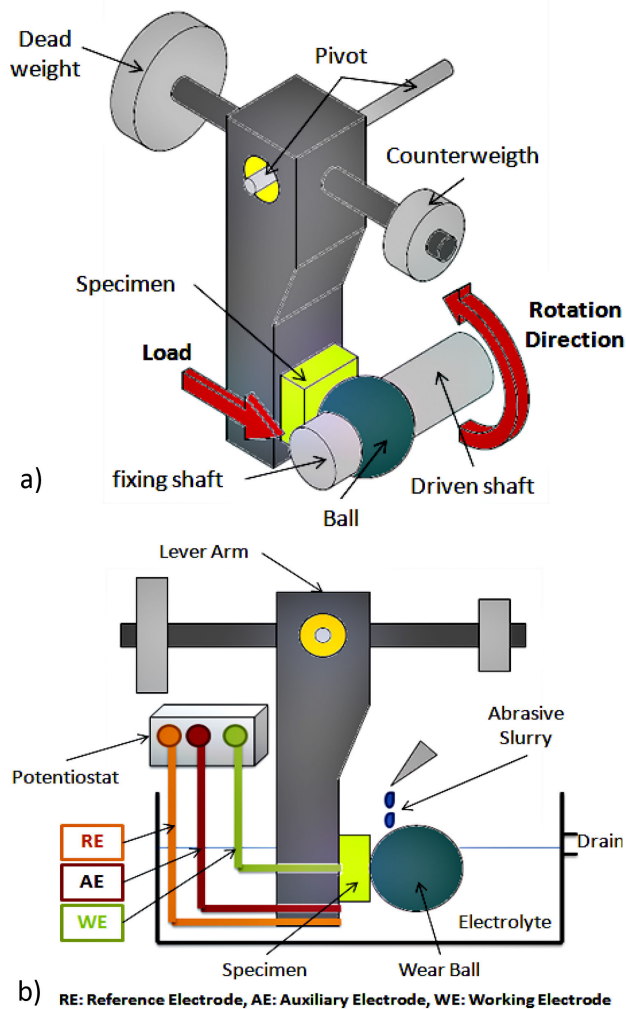


FIGURE 3. Schematics representation of the tests (a) micro-abrasion; (b) micro-abrasion-corrosion.

TABLE I. Chemical composition of AISI 52100 steel.

Element	Fe	C	Cr	Si	Mn	P	S
%	96.924	0.99	1.46	0.21	0.38	0.015	0.021

TABLE II. Chemical composition of the alloy.

Element	Fe	Cr	Ni	Mo	Mn
%	62.89	18.06	14.21	3.12	1.72

To generate simulated biological conditions was used Ringer lactate, which is an isotonic solution for intravenous infusion, similar to the electrolyte composition of the extracellular fluid that provides mineral supplements and water for hydration (6.9 of pH) (see composition Table III) with alumina particles in suspension with 0.3 μm of size.

The evaluated specimens were polished previously until obtain a low surface roughness, which was accomplished using abrasive paper of silicon carbide (SiC), increasing the size from 100 to 1200, and finally polishing the specimens with a

TABLE III. Chemical composition of the electrolyte (Ringer's solution).

Compound	Concentration (g/l)
NaCl	8.6
D-Glucose	0.2
NaHCO3	0.35
Na2HPO4	0.48
KCl	0.4

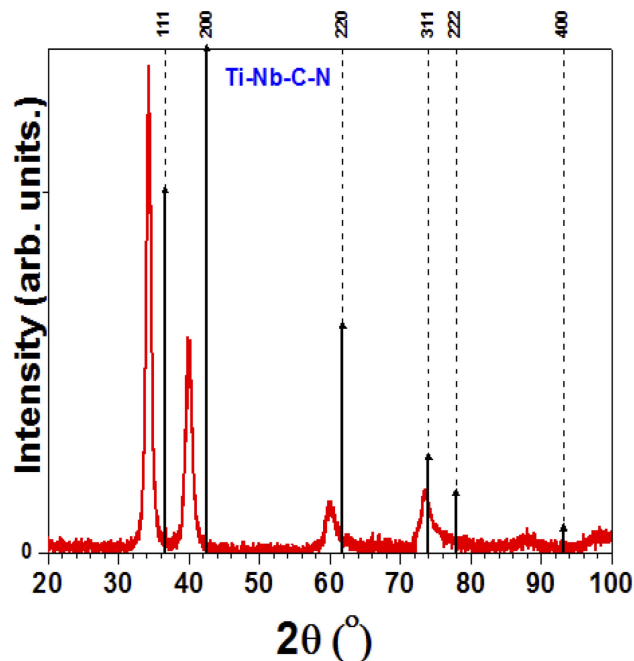


FIGURE 4. XRD pattern for: Ti-Nb-C-N coatings grown with an r.f. negative bias voltages of -20 V. Dash lines indicate the position of the peaks obtained from JCPDF files.

suspensions of alumina (Al<sub>2</sub>O<sub>3</sub>) of 1.0 and 0.05 microns, in a rotating disc. Regarding the multilayer coatings of TiNbCN, were deposited on substrates of stainless steel of 316 LVM by a sputtering technique, denominated reactive magnetron sputtering r.f. (PVD) assisted with negative r.f. polarization voltage applied to the different substrates. Two targets were used: stoichiometric titanium carbide (TiC) and niobium Nb, both of 4 inches (~10 cm) in diameter and ~5 mm thickness, with purity of 99.99%. All substrates are subjected to a cleaning process of their surface of organic contaminants beginning with an ultrasound system, immersed in an ethanol and acetone sequence during 15 minutes for each cycle. Before of the deposition, the vacuum chamber is evacuated by means of mechanical and turbomolecular pump to a base pressure of 7.2 × 10<sup>-5</sup> mbar with the purpose of reduce the residual air effects. Inside the chamber, the substrates are subjected for 15 minutes to a bias voltage of -400 V (r.f.) with a power of 60 W (r.f.) in the plasma of argon (Ar) to remove of the surface other contaminating impurities. The sputtering equip-

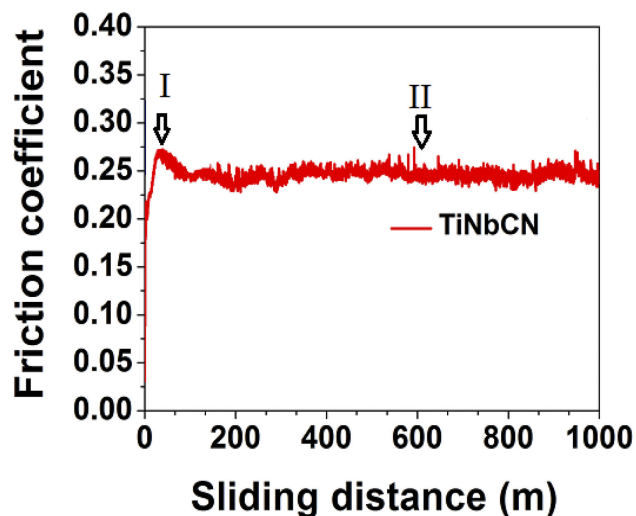


FIGURE 5. Tribological results of TiNbCN coating (friction coefficient as a function of sliding distance).

ment has a substrate positioning system in relation to the target, this parameter allows to vary the bilayer number ( $n$ ) for the present case were 200 bilayers.

The samples were characterized via X-ray diffraction, so the crystal structure of the coatings was determined using a PANALYTICAL X'Pert PRO X-ray diffractometer with Cu K $\alpha$  radiation ( $\lambda = 1.5406 \text{ \AA}$ ) at Bragg-Brentano configuration ( $\theta/2\theta$ ) in high-angle range. The chemical composition of the coatings was determined by energy dispersive X-ray (EDX) analysis using a Philips XL 30 FEG. Analysis of morphological surface before and after of tribological test was carried out by scanning electron microscopy (SEM) Philips XL 30 FEG. Tribological characterization was done by means of Microtest, MT 400-98 tribometer, using a 6 mm

diameter 100Cr6 steel ball like pattern slide. The applied load was 0.5 N with a total running length of 1000 m. The total thickness of the multilayer deposited was approximately 3 microns.

## 4. Results and discussion

### 4.1. Coating Characterization

The Ti-Nb-C-N it was characterized via X-ray diffraction, so the Fig. 5 presents the XRD pattern for the Ti-Nb-C-N coatings grown on silicon (100) with a r.f. negative bias voltages of -20 V. The Bragg peaks of the (1 1 1) and (200) planes for FCC phase are clearly seen indicating the position of the peaks associated to the Ti-Nb-C-N. In the present crystallography model the symmetry of the XRD peaks of quaternary phases suggest that in the monophasic solid solutions, the Ti and Nb atoms occupy the (0,0,0) positions, and C and N atoms the (1/2, 1/2, 1/2) positions of the NaCl-type crystal structure. Also, broadening of the XRD (111), (200), (220) and (311) peaks indicates that solid solutions are obtained with a nanometric grain microstructure. On the other hand, the stoichiometric relationship can be determinate by EDX and lattice parameter of Ti-Nb-C-N coating such as  $\text{Ti}_{0.22}\text{Nb}_{0.78}\text{C}_{0.19}\text{N}_{0.81}$  with  $a_{\text{FCC}(111)} = 0.4303 \text{ nm}$ .

### 4.2. Friction Coefficient Characterization

The friction coefficient value was tested against steel balls and are presented in Fig. 5. This curve showed two distinct stages. In the first stage the friction coefficient, began at a low level 0.8. in the first contact, this stage can be attributed

TABLE IV. Specifications micro-abrasion test (wear only).

Specifications micro-abrasion test (wear only)	
Specimen material	316 LVM steel, TiNbCN n=200 coatings
Sphere material	AISI 52100 steel (25 mm of diameter)
Particles size	Alumina 0.3 $\mu\text{m}$
Solution	Ringer's solution
Abrasive concentration	0.02 %
Rotation speed	20 rpm
Load	2 N
Number of revolutions	50 revolutions
Sliding distance	7.85 m
Slurry feed rate	30 ml/min
Specifications micro-abrasion-corrosion test (wear with corrosion)	
Reference electrode	Ag/AgCl
Auxiliary electrode	Platinum wire
Working electrode	Specimens (316 LVM steel, TiNbCN n=200 coatings)
EIS	Frequency: 10 kHz a 0.1 Hz
Tafel	$\pm 250 \text{ mV}$ a 10 mV/s

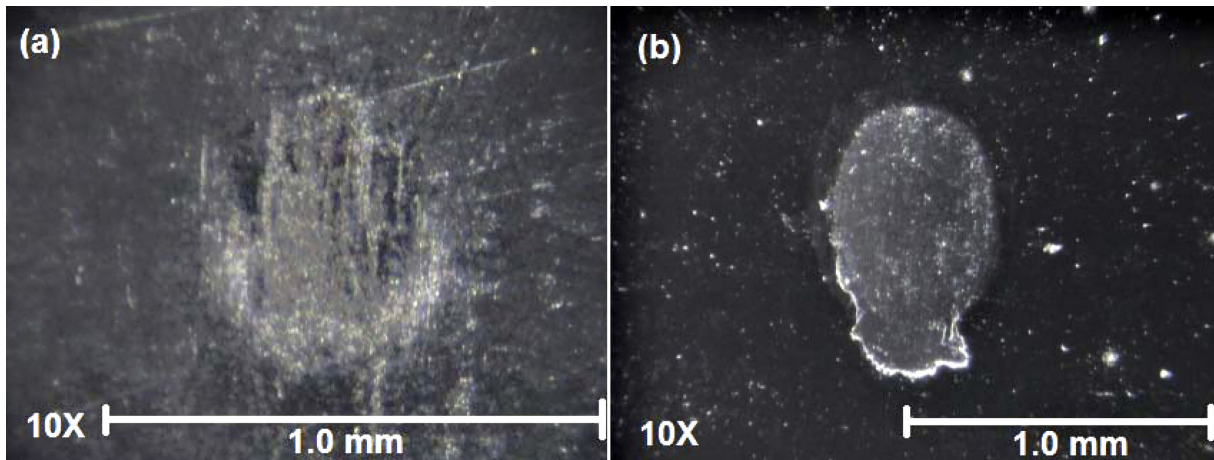


FIGURE 6. Wear scars (a) on the 316 LVM substrate; (b) coated specimen with TiNbCN  $n = 200$ .

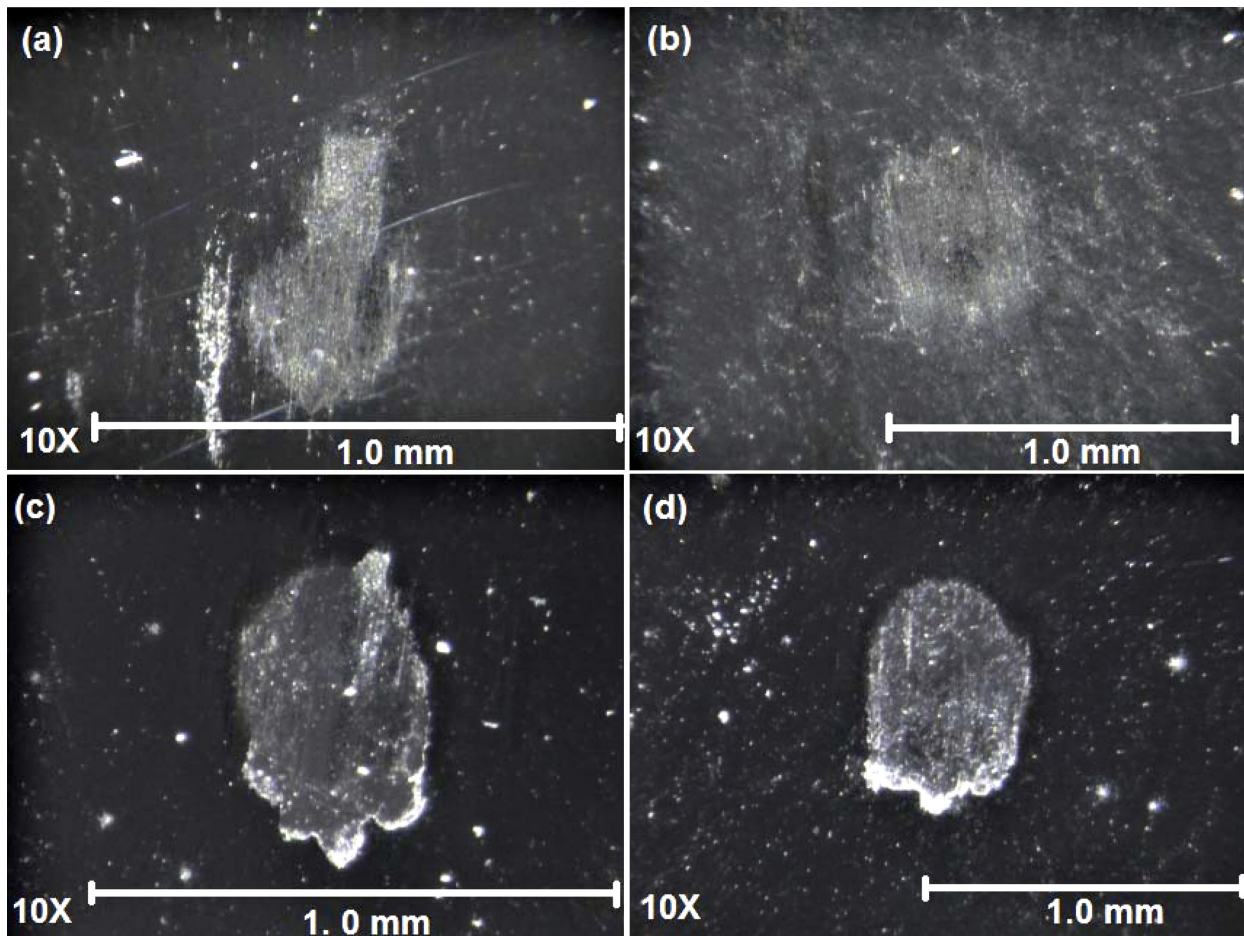


FIGURE 7. Wear scars of the micro-abrasion-corrosion tests by stereographic microscopy: (a) 316 LVM steel substrate subjected to EIS, (b) 316 LVM steel substrate subjected to Tafel, (c) 316 LVM steel substrate coated with TiNbCN  $n = 200$  subjected to EIS, and (d) 316 LVM steel substrate coated with TiNbCN  $n = 200$  subjected to Tafel.

to the running-in period associated with the kind of contact between the steel ball and the coating, in which occurs formation of wear debris by the cracking of roughness tips on both counterparts. This stage has a short time period, then

after that, the friction coefficient increase up to 0.28 followed by a decrease to the friction coefficient of stage II (0.26).

Two types of tests were performed on the substrates and coatings, first tests were performed in which only micro-

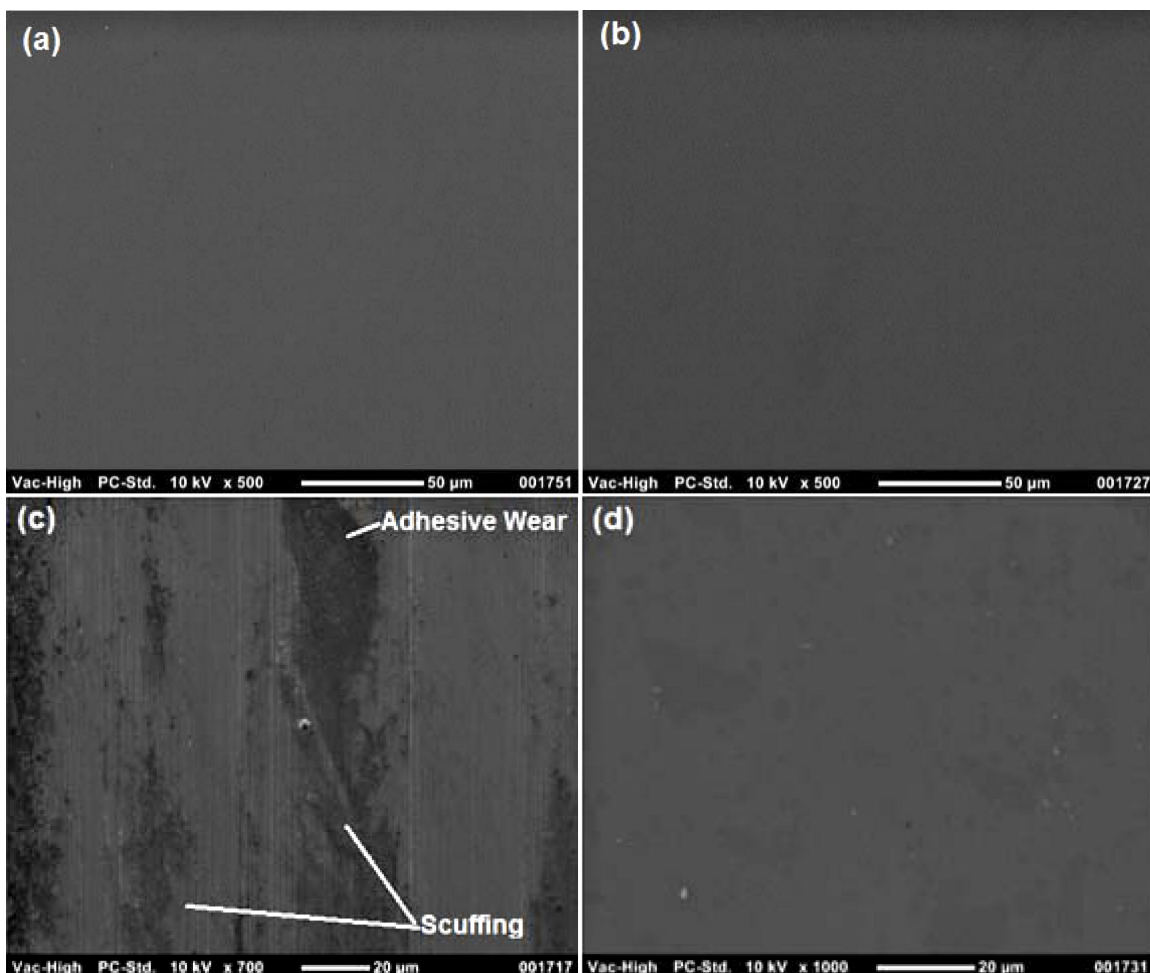


FIGURE 8. Surface of the specimens without micro-mechanism of: (a) 316 LVM steel substrate, (b) 316 LVM steel substrate coated with TiNbCN  $n = 200$ . Wear surface at 50 cycles: (c) 316 LVM steel substrate, (d) 316 LVM steel substrate coated with TiNbCN  $n = 200$ .

abrasive wear was involved, due to it was not used the coupled electrochemical cell. Followed by micro-abrasion-corrosion tests where the wear tests were repeated with the same parameters but using the coupled electrochemical cell, making electrochemical tests such as the Tafel polarization curves and electrochemical impedance spectroscopy (EIS). The used parameters in both types of tests are in the Table IV.

#### 4.3. Stereoscopy and SEM analysis

In the Fig. 6 shows the images of the wear scars taken by a stereoscope at 10 X, where is appreciated the generated lines by the micro-abrasive wear mechanism. Additionally, it is evidenced in Fig. 6b that the coating is totally removed by the action of wear which reaches the substrate.

By including the electrochemical cell in the system no significant changes are observed, like the micro-abrasion test small grooves are seen along the direction of the ball rotation and the removal of the coating, as is shown in the Figs. 7c and 7d.

On the other hand, it was observed the morphology of both the substrate and the coating before and after the

tests using scanning electron microscopy SEM. In the Fig. 8 shows the beginning of the wear mechanism by micro-abrasion, owing to the specimens reveal small grooves in the direction of the particles movement characteristic grooving wear. Comparing the Figs. 8(c) and 8(d) is noticed that the coating protects the substrate even though it is completely removed by the action of micro-abrasive wear, because the 8(d) micrograph does not show the characteristic grooves and it is observed a similar surfaces to the unworn substrate.

In relation to the morphology of the micro-abrasion-corrosion tests, the 316 LVM steel substrates without coating and the substrate coated with TiNbCN  $n = 200$  do not presents large changes, in the substrate is observed pitting corrosion zones and the lines left by the wear associate to the adhesive and micro-abrasion wear (Figs. 9a and 9b), that decreases in the coated system (Figs. 9c and 9b).

#### 4.4. Wear rate estimation

To use the micro-abrasive wear model described above, it was taken the measurements of the scars lengths using SEM, as is

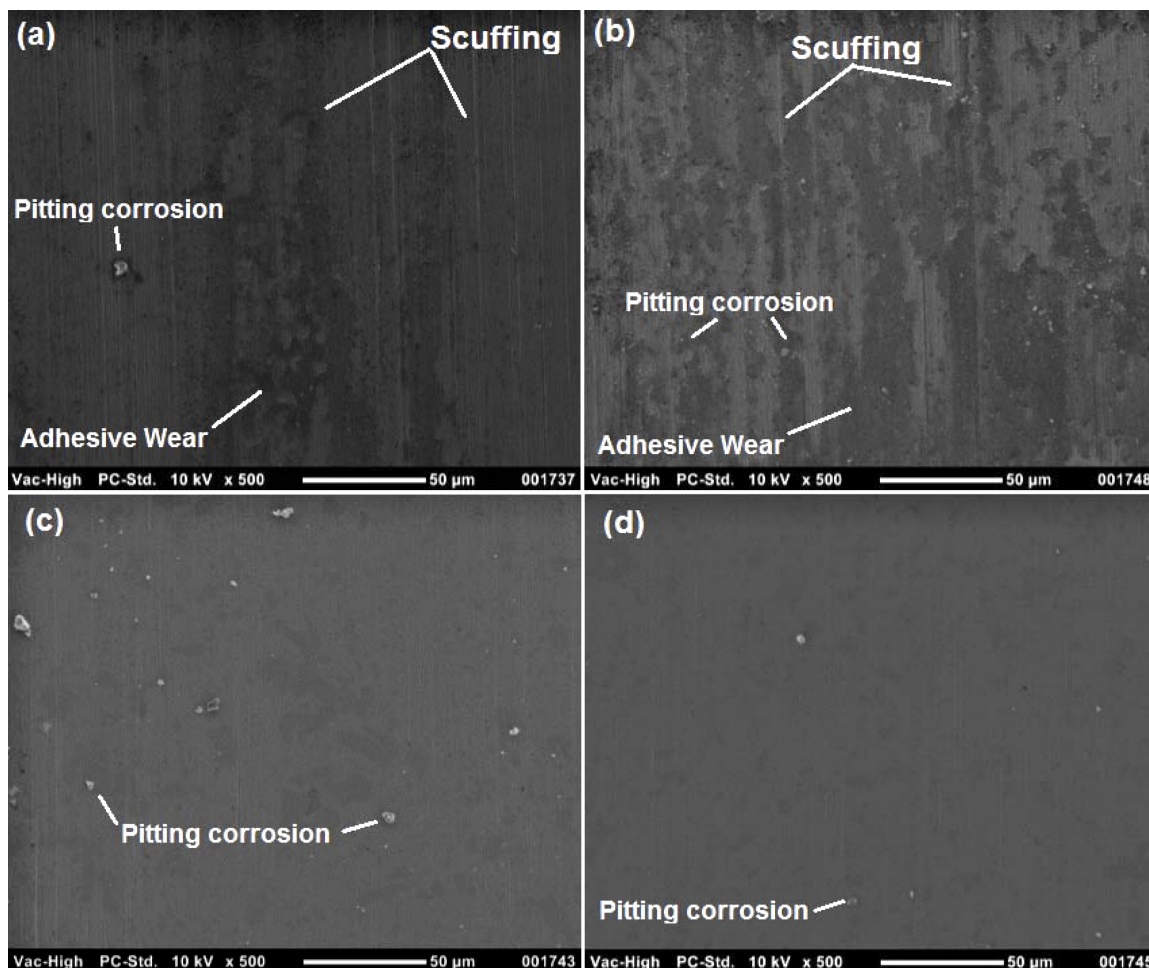


FIGURE 9. Tribo-chemical wear scars by SEM where is observed the adhesive wear, micro-abrasion and pitting corrosion: (a) 316 LVM steel substrate subjected to EIS, (b) 316 LVM steel substrate subjected to Tafel, (c) 316 LVM steel substrate coated with TiNbCN  $n = 200$  subjected to EIS, and (d) 316 LVM steel substrate coated with TiNbCN  $n = 200$  subjected to Tafel.

TABLE V. Length values of the wear scars.

Specimens	Perpendicular length (mm)	Parallel length (mm)	Average length (mm)
(316 LVM) Micro-abrasion	0.54	0.59	0.56
(316 LVM) EIS	0.75	0.70	0.73
(316 LVM) Tafel	0.66	0.48	0.57
(TiNbCN) Micro-abrasion	0.60	0.97	0.79
(TiNbCN) EIS	0.87	0.54	0.71
(TiNbCN) Tafel	0.83	0.60	0.72

observed in the micrographs of the Fig. 10. The length values are listed in the Table V.

With the average lengths, the parameters of normal load (2 N) and the sliding distance (7.85 m) were used the (1) and (3) equations to calculate the volumes and constants of wear for the different preformed tests as is shown in the Table VI. It is important to mention that for the system coating-substrate was not possible to calculate the volumes and constants of

wear separately, due to the material behavior, hence the calculations were performed on the whole system.

In the Fig. 11 is observed the behavior of the specimens plotted with wear constants calculated above. It was evident that the substrate has a better performance when tests are done only micro-abrasive wear. However, when the test was carry out with corrosive phenomena has an increased wear volume by the synergistic effect of (tribo-corrosion). In con-

TABLE VI. Volumes and constants of wear.

Specimens	Wear volumen (mm <sup>3</sup> )	Wear constant (m <sup>2</sup> /N)
(316 LVM) Micro-abrasion	$1.93 \times 10^{-4}$	$1.22 \times 10^{-14}$
(316 LVM) EIS	$2.13 \times 10^{-3}$	$1.35 \times 10^{-13}$
(316 LVM) Tafel	$2.07 \times 10^{-4}$	$1.32 \times 10^{-14}$
(TiNbCN) Micro-abrasion	$7.65 \times 10^{-4}$	$4.87 \times 10^{-14}$
(TiNbCN) EIS	$4.99 \times 10^{-4}$	$3.17 \times 10^{-14}$
(TiNbCN) Tafel	$5.28 \times 10^{-4}$	$3.36 \times 10^{-14}$

TABLE VII. Electrochemical parameters of the substrate and the coating obtained by the micro-abrasion-corrosion system.

	Corrosion Potential E <sub>corr</sub> (V vs Ag/AgCl)	Corrosion Current I <sub>corr</sub> (A/cm <sup>2</sup> )	Corrosion rate (mm/year)
316 LVM steel substrate	-0.097	0.404	229.60
Coating TiNbCN <i>n</i> = 200	-0.250	0.021	11.94

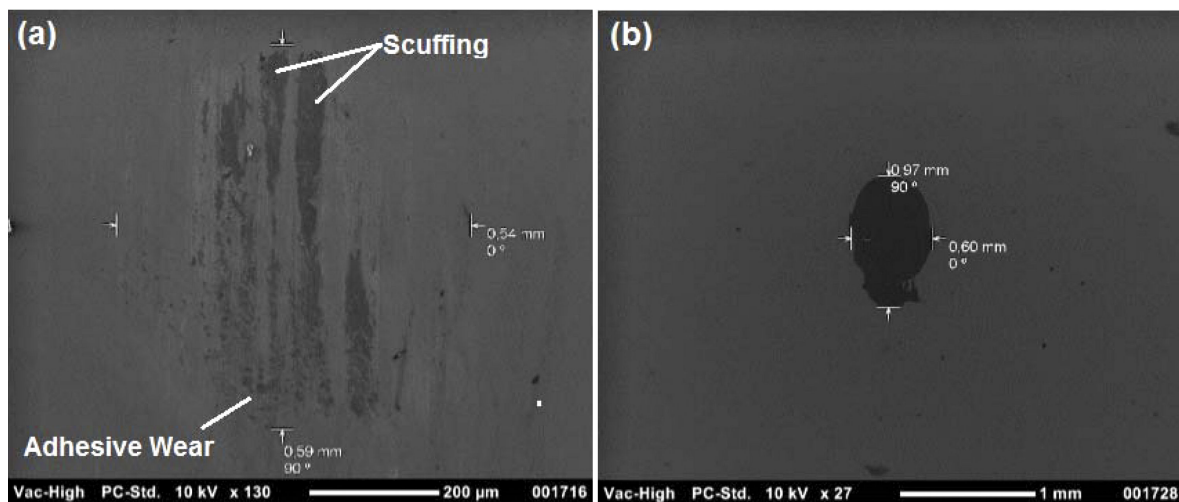


FIGURE 10. SEM micrographs at 50 cycles: (a) the 316 LVM substrate; (b) coated specimen with TiNbCN *n* = 200.

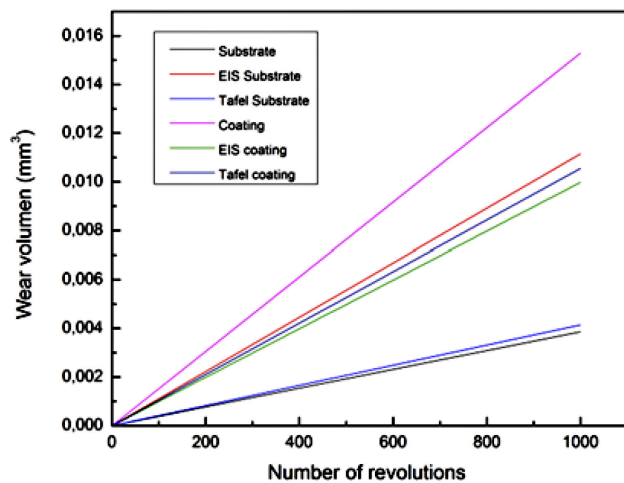


FIGURE 11. Wear volume vs number of revolution: for 316 LVM substrate and 316 LVM substrate coated with TiNbCN *n* = 200, subjected to micro-abrasion-corrosion.

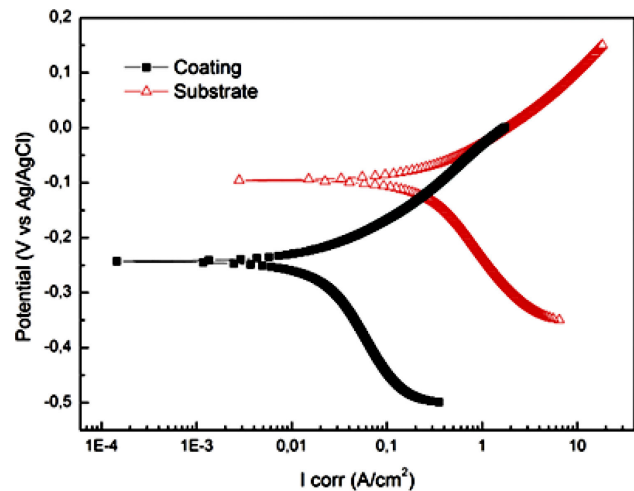


FIGURE 12. Tafel polarization curves, for the 316 LVM substrate and coated specimen with TiNbCN *n* = 200.

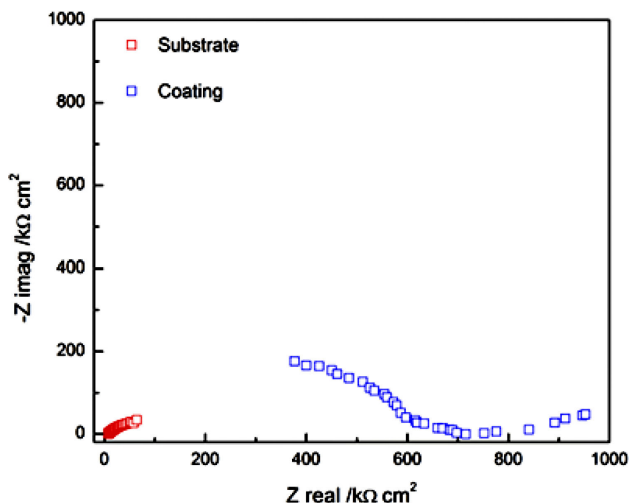


FIGURE 13. Electrochemical impedance spectroscopy (Nyquist diagrams) for the 316 LVM steel substrate and the substrate coated with TiNbCN  $n = 200$ .

trast, the 316 LVM/TiNbCN system presents lower wear volumes when is subjected to a corrosive phenomenon due to the interface that is generated among the substrate and the coating, and the high value of the spatial periodicity ( $\Lambda = 15$  nm).

4.5. Electrochemical tests

4.5.1. Potentiodynamic polarization curves (Tafel)

In the Fig. 12, is observed the Tafel polarization curves of the evaluated substrate and coating. It was obtained a higher corrosion potential for the coated steel, due to the constituents of

the 316LVM alloy, where a protective layer is generated by the chrome that the alloy has. The electrochemical reaction on the protective layer of the titanium niobium carbonitride (TiNbCN), generates corrosion potentials which indicate an adequate performance. Observing the current density values is obtained that the substrate is how promotes a greater tri-chemical wear, in contrast with the multilayer result is acquired a lower value for the protector coating about one order of magnitude, generating a primary protection to the stainless steels.

By extrapolation of the cathodic and anodic slopes were obtained the values of potential, current and corrosion rate (see Table VII).

4.5.2. Nyquist spectrums (EIS)

In the Fig. 13, is observed the Nyquist spectrums, obtained in the combined mechanical and electrochemical test simultaneously, for the substrate is obtained the typical behavior of the AISI 316 LVM steel, since generates two semi-domes which are characteristic of the protective layer and then the material. For the coated steel, the system has a higher value of total impedance in comparison with the substrate owing to the coating that generates an appropriate mechanical (wear resistance) and electrochemical wear protection (corrosion resistance).

Finally, the adjustment of the obtained Nyquist diagrams (Fig. 14) was made by two equivalent circuits. In the Fig. 13a is obtained a circuit, where a parallelism with the performed test is done. Establishing a solution resistance due to the used

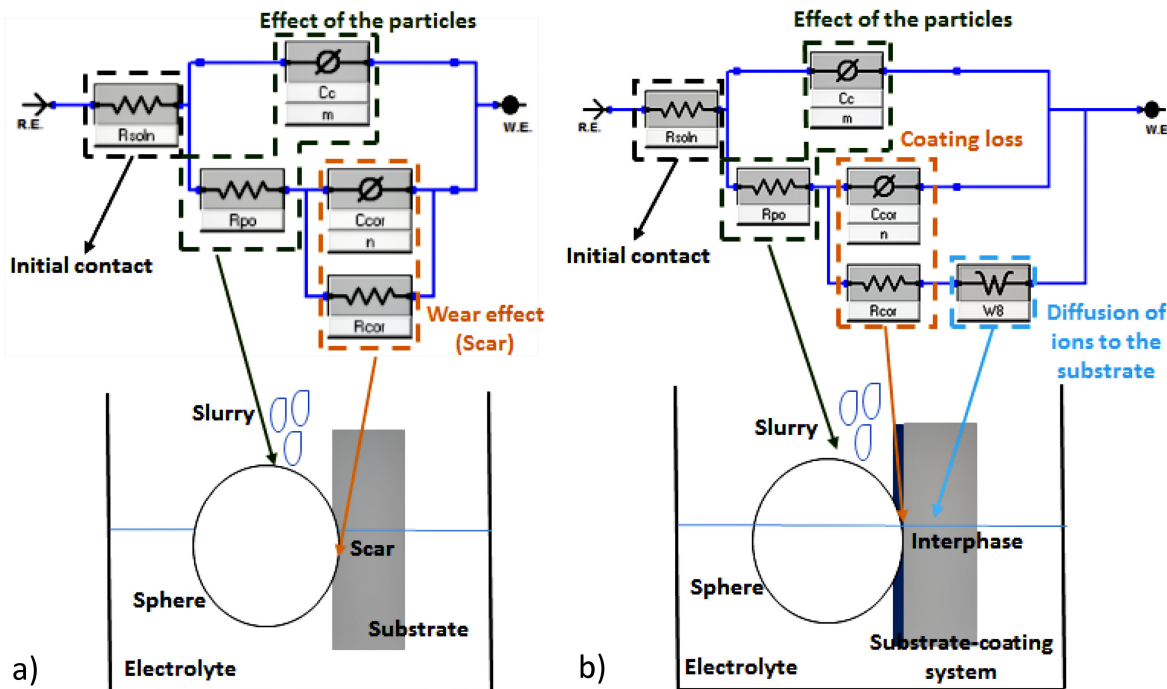


FIGURE 14. Electric circuits of the electrochemical behavior: (a) 316 LVM steel substrate and (b) the substrate coated with TiNbCN  $n = 200$ .

electrolyte, subsequently is determined a resistor in parallel with a CPE element, corresponding to the contact of the sphere with the material. Then, is generated another pair of capacitor resistance owing to the breaking of the protective layer. In the Fig. 14b, it is obtained a circuit with similar parameters to the system described above, with a variation of a Warburg's resistance due to the ions diffusion of the coating to the material denominated 316 LVM substrate.

## 5. Conclusions

A greater effect of micro-abrasion wear was evidenced on the coating in comparison with the substrate, due to the coating presented higher values in terms wear volumes. Additionally, by the observations in the stereoscope and SEM was established that coating was removed at a low number of revolutions with bigger scar dimensions. Nevertheless, analyzing the morphology of the specimens are not observed the small characteristic wear grooves in the coated substrates.

With the electrochemical measurements was observed a better coating performance against corrosion in contrast with

the performed tests at only wear, i.e. that the coated specimens subjected to adhesive wear, micro-abrasive and corrosive phenomena simultaneously, exhibited a reduction of the wear volumes. On the other hand, the substrate increases the presented volumes, which evidences that the coating of TiN-bCN protects the substrate in terms of corrosion resistance.

The protection phenomena of the multilayer can be attributed to the passivating layer generated by the coating and the coating-substrate interface system. Moreover, the high number of interfaces among the layers presents diffusion processes where the coating ions move to the substrate. Demonstrating that such coatings are viable under simulated biological conditions since they improve their performance.

## Acknowledgments

This research was supported by the Universidad Militar Nueva Granada, Bogotá-Colombia project IMP-ING-1767 (2015).

- 
1. J.B. Park, *Biomaterials Science and Engineering*, New York, Plenum Press, (1984) pp. 213.
  2. C.M. Agrawal, *Reconstructing the Human Body Using Biomaterials, JOM*, (1998) 31-35.
  3. ASM International, *Handbook of Materials for Medical Devices*, (2003).
  4. D. Dowson, *Friction and Wear of Medical Implants and Prosthetic Devices, de Friction, Lubrication, and Wear Technology*, Vol ASTM Handbook, *ASTM International*, **18** 1992, pp. 656-664.
  5. C.F. Gutierrez, *Nuevos Materiales Cerámica-Niobio Con Aplicaciones Biomédicas*, Madrid: Tesis Doctoral, Instituto de Ciencia de Materiales de Madrid, (2009).
  6. C. Cácia Ortiz, *Colombia desarrolla prótesis biocompatibles para reducir cirugías* Octubre (2013), <http://www.eltiempo.com/archivo/documento/CMS-13118475> [Online].
  7. A.M. Kaufman, C.I. Alabre, H.E. Rusbash and A. S. Shanbhag, *Journal of Biomedical Materials Research-Part A* **84** (2008) 464-474.
  8. W.N. Capello, J.A. D'Antonio, J.R. Feinberg, M.T. Manley and M. Naughton, *The Journal of Arthroplasty* **23** (2008) 39-43.
  9. J. D'Antonio, W. Capello, M. Manley and B. Bierbaum, *The Journal of Arthroplasty* **17** (2002) 390-397.
  10. S.R. Diwanji, J.K. Seon, E.K. Song and R.T. Yoon, *Clinical Orthopaedics and Related Research* **464** (2007) 242-246.
  11. S.A. Masher, J.D. Lipman, L.J. Curley, M. Gilchrist and T.M. Wright, *Journal of Arthroplasty* **18** (2003) 936-941.
  12. A.P. Serro *et al.*, *Surface & Coatings Technology* **203** (2009) 3701-3707.
  13. S. Calderon, J.C. Sánchez-López, A. Cavaleiro and S. Carvalho, *Journal of the mechanical behavior of biomedical materials*, **41** (2015) 83-91.
  14. P.E. Sinnett-Jones, J.A. Wharton and R.J.K. Wood, *Wear* **259** (2005) 898-909.
  15. J. D'Antonio *et al.*, *Journal of Arthroplasty* **17** (2002) 390-397.
  16. J.P. Garino, *Bioceramics in Joint Arthroplasty. Review of controlled clinical studies with ceramic on ceramic total hip replacements in the United States of America*, ed. H. Zippel and M. Dietrich. 2003, Berlin: Steinkopff Verlag.
  17. Wang Li *et al.*, *Applied surface science* **332** (2015) 1-33.
  18. E. Dunstan *et al.*, *Journal of Bone and Joint Surgery-American* **90A** (2008) 517-522.
  19. H. Pandit, *et al.*, *Journal of Bone and Joint Surgery-British* **90B** (2008) 847-851.
  20. J. Esguerra-Arce *et al.*, *Rev. Mex. Fis.* **60** (2014) 210-216.
  21. J.C. Caicedo, W. Aperador, and Y. Aguilera, *Rev. Mex. Fis.* **59** (2013) 364-373.
  22. I. Saravanan, A. Elaya Perumal, S.C. Vettivel, N. Selvakumar, and A. Baradeswaran, *Materials and Design* **67** (2015) 469-482.
  23. J.C. Caicedo *et al.*, *Applied Surface Science* **256** (2010) 5898-5904.
  24. Ming Zhang, Shengli Ma, Kewei Xu, Long Bai and Paul K. Chu, *Vacuum* **115** (2015) 50-57.
  25. A.P. Serro *et al.*, *Surface & Coatings Technology* **203** (2009) 3701-3707.
  26. M.M. Stack *et al.*, *Wear* **269** (2010) 376-382.

27. M.G. Gee *et al.*, *Ball Cratering or Micro-Abrasion Wear Testing of Coating*, Measurement Good Practice Guide No 57, Teddington, Middlesex, United Kingdom, National Physical Laboratory, (2002).
28. Y.S. Li, K. Wang, P. He, B.X. Huang, P. Kovacs, *J. Raman Spectrosc.* **30** (1999) 97-103.
29. K. L. Rutherford and I. M. Hutchings, *Surface and coatings technology* **79** (1996) 236-237.
30. K. L. Rutherford and I. M. Hutchings, *Journal of Testing and Evaluation* **25** (1997) 250-260.